ELSEVIER

Chemical Engineering Journal 87 (2002) 275–284

Chemical Engineering Journal

www.elsevier.com/locate/cej

A closed-form solution of population-balance models for the dissolution of polydisperse mixtures

Massimiliano Giona [a,*], Alessandra Adrover [a], Francesca Pagnanelli [b], Luigi Toro [b]

[a] *Dipartimento di Ingegneria Chimica, Universitá di Roma "La Sapienza", via Eudossiana 18, 00184 Rome, Italy*
[b] *Dipartimento di Chimica, Universitá di Roma "La Sapienza", piazzale Aldo Moro, 00184 Rome, Italy*

Received 19 February 2001; received in revised form 19 July 2001; accepted 29 August 2001

Abstract

This paper develops a closed-form solution for the population-balance equations describing the dissolution of polydisperse mixtures of spherical particles in the presence of external mass-transfer resistance. The general case, obtained by relaxing the assumption of an excess concentration of fluid reactants, is also considered. In mathematical terms, this leads to a nonlinear first-order functional equation that can be solved by making use of a warped-time transformation. The inclusion of the fragmentation dynamics of solid particles occurring during the chemical dissolution process is also briefly addressed.

Keywords: Closed-form solution; Dissolution; Population-balance equations

1. Introduction

The kinetics of the leaching and dissolution of powdered materials has mainly been examined with reference to a uniform average particle diameter. For nonporous material, classical shrinking-core models have been widely applied to describe the kinetics of leaching processes [1–6].

If the reacting unit is to be scaled up correctly and an accurate distinction drawn between kinetic effects and the structural properties of the solid particles, it is important that nonuniformities in particle size be taken into account. This means that a particle mixture should be described by means of a distribution function (strictly speaking a nonnormalized probability density function) labeled continuously with respect to the particle size (usually the particle radius) and satisfying a population-balance equation [7,8] that takes into account particle shrinking due to dissolution and, if necessary, other physico-chemical phenomena modifying particle size, such as fragmentation.

An in-depth discussion of the numerical methods for approaching population balances—not for dissolution kinetics but for other phenomenologies such as aggregation, nucleation and break-up—is developed by Kumar and Ramkrishna [9–11].

Despite the fact that the dissolution of powdered materials falls into the natural realm of application of population balances and that the assumption of uniform particle size may lead to severe kinetic misinterpretation of the dissolution process, and hence to grossly inappropriate scale-up analyses in the presence of a broad distribution of particle radii [15], very few papers make use of this approach [12–16]. Sepulveda and Herbst [12], and Crundwell and Bryson [14] apply population balances in the analysis of flow reactors at a steady state.

In a series of two papers, Le Blanc and Fogler [15,16] analyze the effects of polydispersity of solid-particle sizes in the batch-dissolution kinetics of powdered minerals. The investigation essentially covers two cases corresponding to kinetic and external film control, assuming a large surplus of fluid reactants and applying particular functional forms of the initial particle-size distribution.

The dissolution kinetics of a polydisperse mixture gives rise mathematically to a first-order partial differential equation for the particle distribution function. We show in this paper that a closed-form solution for this equation can be obtained under fairly general conditions (more general than the cases analyzed by Le Blanc and Fogler) in mixed regimes and for any initial particle size distribution. We also provide a systematic analysis of population-balance equations in leaching processes by relaxing the assumption of excess fluid reactants. The case of fragmentation processes occurring during the dissolution process is also addressed in passing.

* Corresponding author. Tel.: +39-6-445-85-892; fax: +39-6-445-85-339.
E-mail address: max@giona.ing.uniroma1.it (M. Giona).

1385-8947/02/$ – see front matter
PII: S1385-8947(01)00242-X

Nomenclature

$a(x)$	fragmentationrate
$b(x; y)$	numberof fragments of radius x generated by a particle of radius y
c_A	bulkphase solvent concentration
$c_{A,0}$	initialsolvent concentration
$c_{A,s}$	surfacesolvent concentration
D	diffusioncoefficient
k_m	mass-transfercoefficient
k_r	dissolutionrate constant
$\tilde{k}_r$	$\nu_A k_r / M_{w,s}$
$M_{w,s}$	molecularweight of solid reactant
n	reactionorder
$n(x, \theta)$	particledistribution function
$\tilde{n}(x, s)$	Laplacetransform of $n(x, \theta)$
$n_0(x)$	initialparticle distribution function
$n_{s,0}$	numberof moles of solid initially present
r	particleradius
r_{ref}	referenceparticle radius
r_v	definedby Eq. (2.5)
Re	Reynoldsnumber
s	Laplacevariable
Sc	Schmidtnumber
Sh	Sherwoodnumber
t	time
v	characteristicfluid velocity
V_r	reactorvolume
x	r/r_{ref}, dimensionless radius
x_D	definedby Eq. (2.7)
x_v	r_v/r_{ref}, see Eq. (2.4)
$x^*(\theta)$	peaklocation of the distribution $n(x, \theta)$ at time θ
X	conversion
y_A	$c_A/c_{A,0}$

Greek symbols

γ_A	solid-to-liquidstoichiometric loading ratio
ν	kinematicviscosity
ν_A	stoichiometriccoefficient of solvent A
ω	$dx/d\theta$
ρ_s	soliddensity
τ	reactiontime, Eq. (2.7)
τ_w	warpedtime, defined by Eq. (5.2)
θ	dimensionlesstime

This paper is organized as follows. Section 2 describes the physical modeling of the process and introduces the resulting population-balance equation. Section 3 develops the closed-form solution in the case of a large surplus of fluid reactants. Section 4 analyzes several examples for different dissolution regimes and for several forms of model kinetics. Section 5 addresses the solution of the population-balance equation in the case where there is no large surplus of fluid reactant. In this case, the population-balance equation becomes nonlinear and can be formally solved by means of a suitable warped-time transformation. Finally, the concluding section briefly addresses the formal setting of the population-balance equations in the case where fragmentation processes of solid particles are also taken into account.

2. Statement of the problem

Let us consider the isothermal batch-dissolution process of a mixture of nonporous solid particles of spherical shape on the assumption that there is only one limiting reactant A, and that the dissolution kinetics is elementary of order n, i.e. $r(c_A) = k_r c_A^n$. This means that the dissolution of a generic particle follows the equation:

$$\frac{dr}{dt} = -\frac{k_r c_{A,s}^n}{\rho_s}, \tag{2.1}$$

where r is the particle radius. The surface concentration $c_{A,s}$ can be obtained by enforcing film theory, i.e. the equality between the flux across the boundary layer and the rate of consumption due to surface kinetics. Let

$$\text{Solid} + \nu_A A \rightarrow \text{Products} \tag{2.2}$$

be the stoichiometric equation describing dissolution, and let us assume that products dissolve in the liquid phase. For a first-order kinetics[1] ($n = 1$), the surface concentration $c_{A,s}$ is given by

$$c_{A,s} = \left(1 + \frac{\tilde{k}_r}{k_m}\right)^{-1} c_A, \tag{2.3}$$

where c_A is the bulk fluid concentration, $\tilde{k}_r = \nu_A k_r / M_{w,s}$, and k_m the mass-transfer coefficient, which can be expressed by means of the classical correlation for spherical objects:

$$k_m = \frac{D}{2r} Sh = \frac{D}{2r}(2 + a\, Sc^{1/3} Re^{1/2}) = \frac{D}{2r}\left[2 + a\, Sc^{1/3}\left(\frac{2rv}{\nu}\right)^{1/2}\right] = \frac{D}{2r}\left[2 + \left(\frac{r}{r_v}\right)^{1/2}\right], \tag{2.4}$$

where $a = 0.6$ and

$$r_v = \frac{\nu}{2a^2 Sc^{2/3} v}. \tag{2.5}$$

By making use of Eqs. (2.3)–(2.5) and by defining the dimensionless radius $x = r/r_{ref}$, where r_{ref} is some reference value (to be specified below), Eq. (2.1) attains the following form for $n = 1$:

$$\frac{dx}{d\theta} = -y_A \left[1 + \frac{x}{x_D(2 + \sqrt{x/x_v})}\right]^{-1}, \tag{2.6}$$

[1] The case of a nonlinear kinetics is addressed in Section 4.

where

$$y_A = \frac{c_A}{c_{A,0}}, \qquad \tau = \frac{\rho_s r_{ref}}{k_r c_{A,0}}, \qquad \theta = \frac{t}{\tau},$$
$$x_D = \frac{D}{2\tilde{k}_r r_{ref}}, \qquad x_v = \frac{r_v}{r_{ref}}. \tag{2.7}$$

The dimensionless quantity x_v admits the meaning of the reciprocal of an effective Reynolds number referred to the radius r_{ref}, while x_D can be viewed as the reciprocal of the surface square Thiele modulus.

In the case of polydisperse mixtures of spherical particles undergoing chemical dissolution, the balance equation (which is usually referred to as a population balance) for the distribution function $n(x,\theta)$ ($n(x,\theta)\,dx$ is the number of particles possessing a dimensionless radius between x and $x + dx$), is given by

$$\frac{\partial n(x,\theta)}{\partial \theta} + \frac{\partial[\omega(x, y_A) n(x,\theta)]}{\partial x} = 0, \tag{2.8}$$

where

$$\omega(x, y_A) = \frac{dx}{d\theta} = -y_A \left[1 + \frac{x}{x_D(2 + \sqrt{x/x_v})}\right]^{-1} = y_A \omega_0(x), \tag{2.9}$$

equipped with the initial condition:

$$n(x, 0) = n_0(x). \tag{2.10}$$

Two cases should be discussed separately.

Case a: There is a large surplus of reactant A. This means that $y_A \simeq 1$ and the "velocity" ω entering into Eq. (2.8) depends exclusively on x, i.e.

$$\omega = \omega_0(x), \tag{2.11}$$

and the population-balance equation (2.8) is therefore, linear in $n(x,\theta)$. Le Blanc and Fogler [15] address this case exclusively for a first-order reaction. In particular, the case $\omega(x) = -1$ corresponds to a kinetics controlled by surface reaction, while for $x_v \to \infty$, $\omega(x) = -(1 + x/2x_D)^{-1}$ describes dissolution under creeping-flow conditions [16].

Case b: There is no surplus of the reactant A. It follows from stoichiometric equation (2.2) that

$$y_A(\theta) = 1 - \gamma_A \left[1 - \frac{\int_0^\infty x^3 n(x,\theta)\,dx}{\int_0^\infty x^3 n_0(x)\,dx}\right], \tag{2.12}$$

where $\gamma_A = \nu_A n_{s,0}/V_r c_{A,0}$, V_r is the reactor volume, takes into account the loading ratio of the solid and the fluid reactant. In this case, the population-balance equation is nonlinear in $n(x,\theta)$ due to the dependence of $y_A(\theta)$ on the overall mass of the solid mixture at time θ. It is important to observe that this nonlinear contribution depends exclusively on an integral functional of $n(x,\theta)$.

The solution of Eq. (2.8) in Case (a) will be developed in the following section, while Section 5 tackles the solution in Case (b).

It is useful to observe that the overall quantities describing the extent of the reaction are linear functionals of $n(x,\theta)$. In particular, the conversion X is proportional to the third-order moment of the distribution

$$X(\theta) = 1 - \frac{\int_0^\infty x^3 n(x,\theta)\,dx}{\int_0^\infty x^3 n_0(x)\,dx}, \tag{2.13}$$

while the wetted surface area per unit mass θ is proportional to the second-order moment.

3. Closed-form solution

The analysis of Eq. (2.8) in the case of kinetic control and in the mass-transfer controlled case (for $y_A = 1$) is developed by Le Blanc and Fogler [15,16] for some particular initial distributions $n_0(x)$, and essentially for a log-normal distribution.

It is indeed possible to obtain a formal solution of Eq. (2.8) in the more general case and for generic initial distributions. This section briefly addresses this issue by considering a first-order reaction $n = 1$ on the assumption $y_A = 1$ (Case a). The solution of this case is the starting point for obtaining the general solution in the case of nonlinear kinetics (Section 4) and in Case b (Section 5).

Under this hypothesis, Eq. (2.8) is linear in $n(x,\theta)$ and it is convenient to introduce the Laplace transform $\hat{n}(x,s)$ of the distribution function:

$$\hat{n}(x,s) = \int_0^\infty n(x,\theta)\, e^{-s\theta}\, d\theta, \tag{3.1}$$

so that Eq. (2.8) becomes

$$s\hat{n}(x,s) - n_0(x) + \frac{d[\omega_0(x)\hat{n}(x,s)]}{dx} = 0. \tag{3.2}$$

It should be noted that $n(x,\theta)$ is defined mathematically for $x \in (-\infty, \infty)$ even though, for kinetic purposes, only positive values of x admit a physical meaning. Consequently, Eq. (3.2) is not equipped with any boundary condition, and the regularity of the solution should be only enforced for $|x| \to \infty$.

The introduction of the auxiliary function $g(x,s) = \omega_0(x)\hat{n}(x,s)$ causes Eq. (3.2) to take the following form:

$$\frac{dg(x,s)}{dx} = -\frac{s}{\omega_0(x)} g(x,s) + n_0(x), \tag{3.3}$$

the general solution of which is given by

$$g(x,s) = C \exp\left(-s\int_0^x \frac{dz}{\omega_0(z)}\right) + \int_0^x n_0(y) \exp\left(-s\int_y^x \frac{dz}{\omega_0(z)}\right) dy. \tag{3.4}$$

Due to the regularity condition for $|x| \to \infty$, the constant C is identically vanishing, so that the Laplace transform of

$n(x,\theta)$ is given by

$$\hat{n}(x,s) = \frac{1}{\omega_0(x)} \int_0^x n_0(y) \exp[-s(h(x)-h(y))]\,\mathrm{d}y, \tag{3.5}$$

where

$$h(x) = \int_0^x \frac{\mathrm{d}z}{\omega_0(z)}. \tag{3.6}$$

The inverse Laplace transform of Eq. (3.5) attains the following form:

$$\begin{aligned} n(x,\theta) &= \frac{1}{\omega_0(x)} \int_0^x n_0(y)\delta(\theta - h(x) + h(y))\,\mathrm{d}y \\ &= \frac{\omega_0(h^{-1}(h(x)-\theta))}{\omega_0(x)} n_0(h^{-1}(h(x)-\theta)), \end{aligned} \tag{3.7}$$

where h^{-1} is the inverse of the monotonic function $h(x)$ defined by Eq. (3.6), and $\delta(x-x_c)$ is Dirac's delta-distribution centered at $x = x_c$. Eq. (3.7) is the formal general solution of Eq. (2.8). The following section addresses some specific cases of kinetic interest.

4. Examples and discussion

This section develops several particular cases of the application of Eq. (3.7), also extending the analysis to nonlinear kinetics.

4.1. First-order kinetics

For a first-order kinetics, the auxiliary function $h(x)$ is given by

$$\begin{aligned} h(x) &= -\int_0^x \left[1 + \frac{\xi}{x_D(2+\sqrt{\xi/x_v})}\right] \mathrm{d}\xi \\ &= -x - \frac{2\sqrt{x_v}}{x_D}\left[\frac{x^{3/2}}{3} - x\sqrt{x_v} + 4x_v\sqrt{x}\right. \\ &\quad \left. -8x_v^{3/2}\log\left(\frac{\sqrt{x}+2\sqrt{x_v}}{2\sqrt{x_v}}\right)\right]. \end{aligned} \tag{4.1}$$

Several cases are of interest. The limit $x_D \to \infty$ corresponds to kinetic control. In this case, $\omega_0 = -1$, $h(x) = h^{-1}(x) = -x$, so that Eq. (3.7) becomes

$$n(x,\theta) = n_0(x+\theta). \tag{4.2}$$

The initial distribution translates in a parallel way along the x-axis towards lower values of x as time increases. If it possesses initial radii lower than a prescribed value x_m, i.e. if $n_0(x)$ admits a compact support ($n_0(x) = 0$ for $x > x_m$), complete consumption occurs for $\theta > x_m$.

Another particular case of interest is that of creeping-flow conditions, corresponding to $Re \to 0$ and $x_v \to \infty$. In this case, $\omega_0(x) = -(1 + x/2x_D)^{-1}$ and

$$\begin{aligned} h(x) &= -\left(x + \frac{x^2}{4x_D}\right), \\ h^{-1}(x) &= -2x_D + [4x_D^2 - 4x_D x]^{1/2}, \end{aligned} \tag{4.3}$$

so that

$$h^{-1}(h(x)-\theta) = -2x_D + [(x+2x_D)^2 + 4x_D\theta]^{1/2}. \tag{4.4}$$

The substitution of Eq. (4.4) into Eq. (3.7) yields

$$\begin{aligned} n(x,\theta) &= \frac{2x_D + x}{[(x+2x_D)^2 + 4x_D\theta]^{1/2}} \\ &\quad \times n_0(-2x_D + [(x+2x_D)^2 + 4x_D\theta]^{1/2}), \end{aligned} \tag{4.5}$$

which was obtained by Le Blanc and Fogler [16] in the particular case of an initial log-normal distribution.

In the general case of a first-order dissolution kinetics, the expression for the inverse function $h^{-1}(x)$ entering into Eq. (3.7) cannot be made explicit. This is, however, a minor issue since h^{-1} can be obtained from Eq. (4.1) by points and, upon interpolation, substituted into Eq. (3.7).

Throughout this paper, we consider an initial distribution possessing a bounded maximum radius r_{max}, such that $n_0(r) = 0$ for $r > r_{max}$. In this case, the reference radius r_{ref} can be chosen to be equal to r_{max}, so that $n_0(x)$ is different from zero in the unit interval $x \in [0,1]$. This means that $h : [0,1] \to [-H, 0]$, where $H > 0$ and $h^{-1} : [-H, 0] \to [0,1]$. The assumption of compact support of the initial distribution, which is wholly reasonable in all the cases of physical interest, simplifies the computation of Eq. (3.7) since both the auxiliary functions h and h^{-1} can be tabulated on an arbitrarily fine grid and stored in an array structure, thus simplifying the computation of the quantity $h^{-1}(h(x)-\theta)$ in all the cases where it is impossible to express either h or h^{-1} or both of them by means of elementary functions.

As a case study, we consider an initial particle population distributed according to a modified Gamma distribution:

$$n_0(x) = \begin{cases} Cx^{\nu_0}(1-x)^{\nu_1}\exp(-\beta x), & x \in [0,1], \\ 0 & \text{elsewhere}, \end{cases} \tag{4.6}$$

where $\nu_0 > -1$, $\nu_1 > 0$, $\beta > 0$, and $C > 0$, which is very flexible and gives rise to a broad phenomenology of initial distributions by changing ν_0, ν_1 and β. This distribution vanishes for $x = 1$, and for $x = 0$ if $\nu_0 > 0$. If $\nu_0 > 0$, this class of functions possesses unimodular behavior characterized by a single local maximum centered at $x_0^* = (\beta + \nu_0 + \nu_1 - \sqrt{(\beta+\nu_0+\nu_1)^2 - 4\beta\nu_0})/2\beta$. The prefactor C depends on the total volume (mass) of the particle ensemble. Henceforth, we assume

$$C = C_0\left[\int_0^1 x^{\nu_0+3}(1-x)^{\nu_1}\exp(-\beta x)\,\mathrm{d}x\right]^{-1} \tag{4.7}$$

for a fixed value of the constant C_0, say $C_0 = 1$, which ensures an overall dimensionless mass equal to $\frac{1}{3}4\pi\rho_s C_0$.

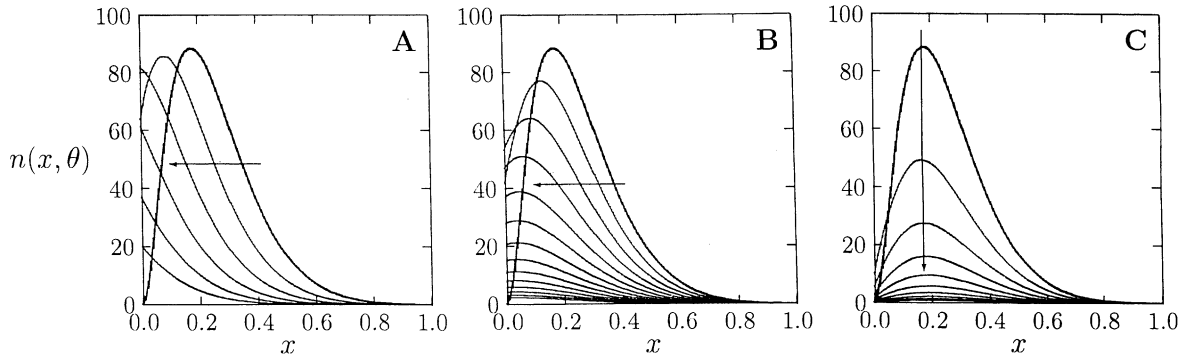

Fig. 1. Particle distribution $n(x,\theta)$ at several time instants (sampling time $\Delta\theta$) for $\nu_0 = 2$, $\nu_1 = 1$, $\beta = 10$ (distribution I) and $x_v = 1$. The bold line corresponds to the initial distribution. The arrow indicates increasing values of time θ spanning the conversion range from $X = 0$ to about 0.98: (A) $x_D = 1$, $\Delta\theta = 10^{-1}$; (B) $x_D = 10^{-1}$, $\Delta\theta = 10^{-1}$; (C) $x_D = 10^{-2}$, $\Delta\theta = 1$.

The dissolution kinetics depends on two parameters, x_D and x_v, corresponding to the reciprocal of effective square Thiele and Reynolds numbers, and on the shape of the initial distribution function.

We consider two characteristic shapes of the initial distribution: the case of an initial mixture formed by relatively small particles in relation to the reference radius r_{ref}, corresponding to $\nu_0 = 2$, $\nu_1 = 1$ and $\beta = 10$ (henceforth referred to as distribution I) and the opposite case of an initial ensemble essentially composed of large particles and corresponding to $\nu_0 = 10$, $\nu_1 = 1$ and $\beta = 2$ (henceforth referred to as distribution II).

Let us first consider the influence of x_D for a fixed value of $x_v = 1$. Figs. 1 and 2 show the behavior of the particle distribution function for $x_D = 1$ (A), 10^{-1} (B) and 10^{-2} (C), respectively, for distributions I and II. The distributions are sampled at constant time intervals $\Delta\theta$, depending on x_D, in such a way that the most significant range of conversions X from 0 up to 0.98, is covered. The initial distribution is shown by a bold line.

In the case $x_D = 1$ (part A of Figs. 1 and 2), both distributions translate towards lower values of x as the height of the local maximum gradually decreases. For $x_D = 1$, the characteristic times for reaction and mass transfer are comparable to each other, and the behavior of $n(x,\theta)$ is qualitatively close to the case of strict kinetic control, $x_D \to \infty$, Eq. (4.2), corresponding to a rigid translation of $n(x,\theta)$ along the x-axis.

By decreasing x_D, the process becomes progressively controlled by external mass transfer (parts B and C of Figs. 1 and 2). The case $x_D = 10^{-2}$ is particularly interesting. Distribution I (Fig. 1C) qualitatively follows the behavior observed by Le Blanc and Fogler for a log-normal distribution in the mass-transfer controlled case, as was to be expected because distribution I and the log-normal distribution are fairly similar. Phenomenologically, the abscissa $x^*(\theta)$ at which $n(x,\theta)$ attains its absolute maximum does not move appreciably away from its initial location x_0^*, at least for values of the conversion up to $X = 0.98$, and the whole distribution sinks progressively. Conversely, distribution II displays a complete different behavior (Fig. 2C): the distribution translates towards lower values of x, and so does $x^*(\theta)$ starting from a value close to 1 up to 0.

The behavior of the distribution dynamics can be described in a lumped way by considering the time-behavior of $x^*(\theta)$, the abscissa of the absolute maximum. It is

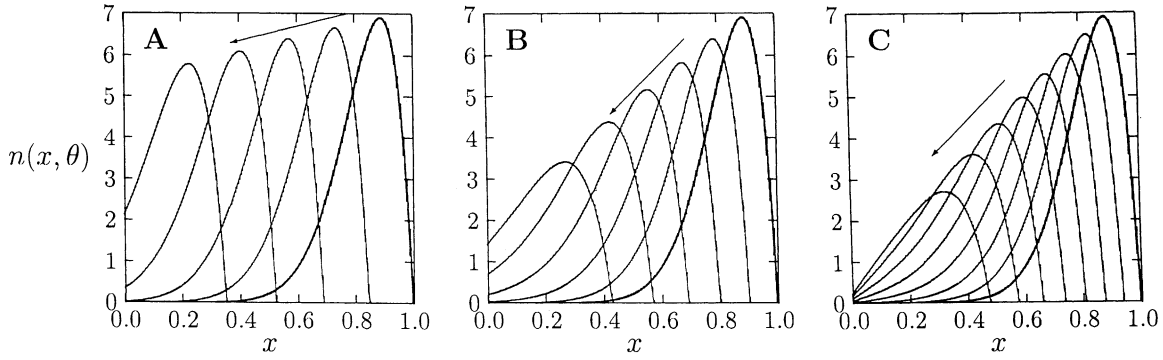

Fig. 2. Particle distribution $n(x,\theta)$ at several time instants for $\nu_0 = 10$, $\nu_1 = 1$, $\beta = 2$ (distribution II) and $x_v = 1$. The bold line corresponds to the initial distribution. The arrow indicates increasing values of time θ spanning the conversion range from $X = 0$ to about 0.98: (A) $x_D = 1$, $\Delta\theta = 2 \times 10^{-1}$; (B) $x_D = 10^{-1}$, $\Delta\theta = 4 \times 10^{-1}$; (C) $x_D = 10^{-2}$, $\Delta\theta = 2$.

convenient to introduce an approximation, valid exclusively in the mass-transfer controlled case, by assuming $x/x_D \geq 1$ and overlooking the contribution due to agitation $x_v \to \infty$. The first inequality is intrinsically an approximation that fails for very small particles $x \ll x_D$. If x_D is small enough, however, the contribution on left-hand side tail of the distribution to the overall dynamics is fairly negligible. On this assumption, the dimensionless shrinking velocity becomes $\omega(x) = -[x/2x_D]^{-1}$, and $h(x) = -x^2/4x_D$, $h^{-1}(x) = \sqrt{-4x_D x}$ and $\alpha(x,\theta) = h^{-1}(h(x) - \theta) = \sqrt{x^2 + 4x_D\theta}$. Eq. (3.7) thus becomes

$$n(x,\theta) = \frac{x}{\sqrt{x^2 + 4x_D\theta}} n_0\left(\sqrt{x^2 + 4x_D\theta}\right) = \frac{x n_0(\alpha(x,\theta))}{\alpha(x,\theta)}. \tag{4.8}$$

The position $x^*(\theta)$ of the maximum fulfills the condition $(\partial n(x,\theta)/\partial x)|_{x=x^*(\theta)} = 0$. By applying Eq. (4.8), this condition can be expressed with respect to the auxiliary function α as follows:

$$4x_D\theta + (\alpha^{*2} - 4x_D\theta)\alpha^* \left.\frac{\mathrm{dlog}\, n_0(\alpha)}{\mathrm{d}\alpha}\right|_{\alpha=\alpha^*} = 0, \tag{4.9}$$

where $x^{*2} = \alpha^{*2} - 4x_D\theta$, i.e.

$$4x_D\theta = \frac{\alpha^{*3}\,\mathrm{dlog}\, n_0(\alpha^*)/\mathrm{d}\alpha}{\alpha^*\,\mathrm{dlog}\, n_0(\alpha^*)/\mathrm{d}\alpha - 1}, \tag{4.10}$$

where $\mathrm{dlog}\, n_0(\alpha^*)/\mathrm{d}\alpha = \mathrm{dlog}\, n_0(\alpha)/\mathrm{d}\alpha|_{\alpha=\alpha^*}$. Eq. (4.10) can be used to determine the position of the maximum quite simply since it returns the graph of θ vs. α^*. By enforcing the definition of x^* as a function of α^* and θ, the graph of x^* vs. θ is readily obtained. Fig. 3 shows the graph of $x^*(\theta)$ vs. the conversion $X(\theta)$ obtained from Eq. (4.10) for the approximate model and compared with the maxima of the complete solution (in which no approximations are made) in the case of the two distributions considered.

This representation of distribution dynamics is particularly convenient for analyzing experimental data since both x^* and X are experimentally measurable quantities.

As can be observed, distribution I for $x_D = 10^{-2}$ and $x_v = 1$ (curve a of Fig. 3A) is characterized by a highly nonmonotonic behavior of $x^*(\theta)$ as a function of the conversion $X(\theta)$. For small $X < 0.4$, x^* decreases as a function of the conversion, reaches a local minimum, and then increases until X reaches values close to 1. Near complete solid consumption, there is a sudden collapse of x^* up to $x^* = 0$. The excursion range over which x^* varies is, however, a narrow interval centered at the initial value x_0^*, for X in the interval $[0, 0.99]$. The approximate model equation (4.10) (curve e in Fig. 3) possesses the same qualitative behavior, although the values attained by x^* are different. This is quite reasonable since Eq. (4.10) holds in the limit of $x_v \to \infty$ and for small values of x_D. As shown by curves (b)–(d) of Fig. 4, the results obtained by decreasing x_D and increasing x_v approach curve (e), i.e. Eq. (4.10).

Fig. 3B shows the dynamics of x^* for distribution II. The solid curve refers to Eq. (4.10), while dots are the values pertaining to the nonapproximate solution for $x_D = 10^{-2}$ and $x_v = 1$. In this case, x^* is a strictly monotonically decreasing function of X tending to 0 for $X \to 1$, thus confirming the qualitative behavior of $n(x,\theta)$ shown in Fig. 2C. In the case of distribution II, the behavior at $x_D = 10^{-2}$ and $x_v = 1$ is already practically indistinguishable from the approximate solution equation (4.10), and a further increase in x_v and/or decrease in x_D makes no appreciable difference to the dynamics of the particle ensemble.

These results demonstrate that the dynamics of particle distributions in the mass-transfer controlled case may give rise to a rich phenomenology that is strongly dependent on the shape of the initial distribution function.

Incidentally, Fig. 3 also addresses the influence of x_v on the dynamics of distribution function. This parameter

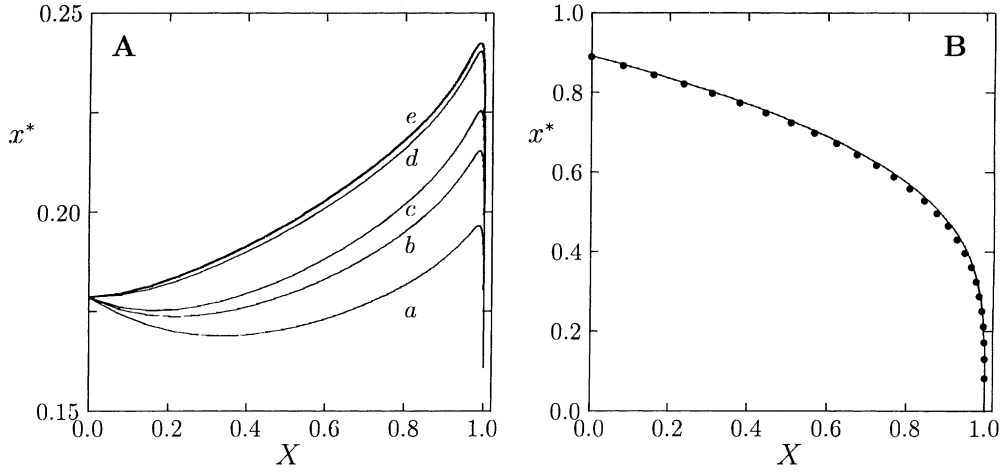

Fig. 3. x^* vs. conversion X. (A) Initial distribution I: (a) $x_v = 1$, $x_D = 10^{-2}$; (b) $x_v = 10$, $x_D = 10^{-2}$; (c) $x_v = 10^3$, $x_D = 10^{-2}$; (d) $x_v = 10^3$, $x_D = 10^{-3}$; (e) Eq. (4.10). (B) Initial distribution II. The solid line corresponds to Eq. (4.10) and the dots refer to $x_v = 1$, $x_D = 10^{-2}$.

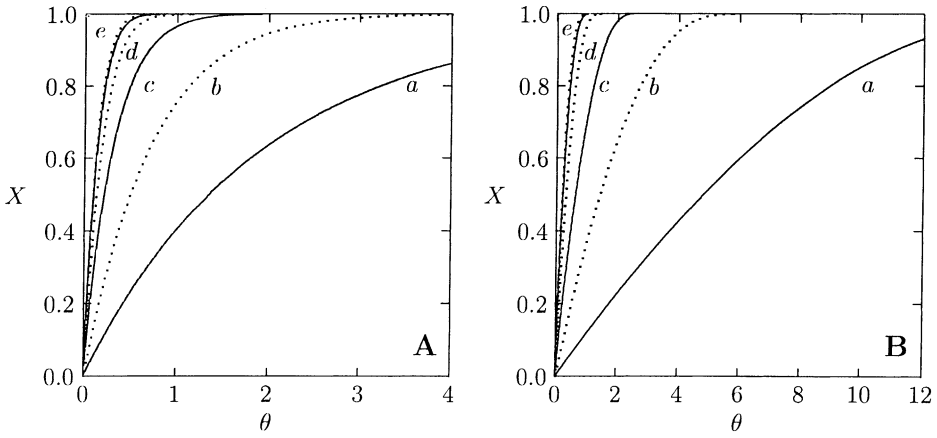

Fig. 4. Conversion–time curves for $x_v = 1$ (continuous lines), and $x_v = 10^{-2}$ (dotted lines). (A) Initial distribution I: (a) and (b) $x_D = 10^{-2}$; (c) and (d) $x_D = 10^{-1}$; (e) $x_D = 1$. (B) Initial distribution II: (a) and (b) $x_D = 10^{-2}$; (c) and (d) $x_D = 10^{-1}$; (e) $x_D = 1$.

takes into account the effect of agitation—as it regards mass transfer—on the dissolution behavior.

Elementary physical considerations and order of magnitude analyses suggest that the influence of x_v becomes more significant for small values of x_D, i.e. in the mass-transfer controlled case, since the effect of agitation may compensate the low value of diffusivity, thus increasing mass transfer. This phenomenon is shown in Fig. 4A and B for distributions I and II, respectively, by considering the overall conversion–time curve. The solid lines refer to $x_v = 1$ and the dotted lines to $x_v = 10^{-2}$.

For high values of $x_D \geq 1$, corresponding to the reaction controlled case, and up to the condition $x_D \simeq 1$, at which the characteristic time for reaction and mass transfer are of the same order of magnitude, the influence of x_v is negligible. Curve (e) shows the almost perfect matching of the conversion–time curves for $x_v = 1$ and 10^{-2}. For lower values of x_D, the effects of agitation cannot be overlooked. For example, for distribution II at $x_D = 10^{-2}$ (Fig. 4B, curves a and b), there is a difference of almost one order of magnitude in the value of the time required to achieve conversion of $X = 0.95$ by changing x_v from 1 to 10^{-2}.

4.2. Nonlinear dissolution kinetics

The case of a nonlinear dissolution kinetics makes no significant difference to the formal structure of the solution expressed by Eq. (3.7) for a first-order kinetics. To show this, we consider an nth order elementary reaction, although the same approach can be extended to any form of rate law.

For an nth order kinetics, the surface concentration $c_{A,s}$ can be obtained from the balance equation

$$k_m(c_A - c_{A,s}) = \tilde{k}_r c_{A,s}^n, \tag{4.11}$$

i.e.

$$y_A - y_{A,s} = \phi^2 y_{A,s}^n, \tag{4.12}$$

where $\phi^2 = \tilde{k}_r c_{A,0}^{n-1}/k_m$ is the square surface Thiele number. Eq. (4.12) can be made explicit with respect to $y_{A,s}$:

$$y_{A,s} = \psi(y_A; \phi^2), \tag{4.13}$$

although the expression for the function ψ cannot be made explicit through elementary functions. The substitution of Eq. (4.13) into Eq. (2.1) yields

$$\frac{dx}{d\theta} = -\psi^n(y_A, \phi^2), \tag{4.14}$$

where the surface Thiele number depends on x because of Eq. (2.4):

$$\phi^2 = \frac{x/x_D}{2 + \sqrt{x/x_v}}, \tag{4.15}$$

where for an nth order kinetics, $x_D = D/2\tilde{k}_r c_{A,0}^{n-1} r_{ref}$.

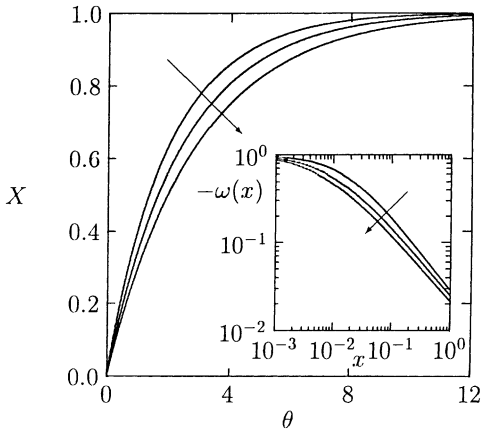

Fig. 5. Conversion–time curves for distribution I in the mass-transfer controlled regime ($x_D = 10^{-2}$, $x_v = 1$) for increasing values of the order of reaction $n = 1, 2, 3$ (indicated by the arrow). The inset shows the corresponding behavior of $-\omega = -\omega_0(x)$.

If there is a large surplus of fluid reactant with respect to the solid, $y_A \simeq 1$ and Eq. (4.14) becomes

$$\frac{dx}{d\theta} = \omega_0(x) = -\psi^n\left(1, \frac{x}{x_D(2+\sqrt{x/x_v})}\right). \tag{4.16}$$

This means that the formal closed-form solution of the population-balance equation is identical to the case of a first-order kinetics, with the only difference that the dimensionless shrinking velocity is now expressed by Eq. (4.16).

Fig. 5 shows the conversion–time curves and the corresponding shrinking velocity profiles $\omega_0(x)$ in the diffusion-controlled regime ($x_D = 10^{-2}$, $x_v = 1$) for distribution I and $n = 1, 2, 3$. As expected, for fixed x_v and x_D, the reaction becomes slower as the order of the reaction increases.

5. Warped time and the influence of fluid reactant concentration

In the case where there is no surplus of the fluid reactant A with respect to the solid, its concentration decreases progressively during the reaction, thus influencing the dissolution process. In this case, the resulting population-balance equation is no longer linear and attains the form of a nonlinear functional equation, as discussed in Section 2.

From Eqs. (2.8), (2.9) and (2.12), it follows that the governing equation expressing the time evolution of the distribution function is given by

$$\frac{\partial n(x,\theta)}{\partial \theta} + y_A(\theta)\frac{\partial[\omega_0(x)n(x,\theta)]}{\partial x} = 0, \tag{5.1}$$

where $y_A(\theta)$ depends exclusively on time θ and is given by Eq. (2.12).

The particular functional form of Eq. (5.1) is suitable for approach by means of a warped-time transformation. Warped-time transformations are widely adopted in reaction engineering, e.g. in connection with the kinetics of continuous mixtures [17,18], and for analyzing the dynamics of lamellar systems in order to model the influence of mixing and/or premixing conditions on the reaction evolutions in stirred systems [19,20].

Let us introduce the following warped-time transformation:

$$\tau_w = \int_0^\theta y_A(\theta')\,d\theta' = \mathcal{F}_w(\theta), \tag{5.2}$$

so that Eq. (5.1) becomes formally identical to Eq. (2.8):

$$\frac{\partial n_w(x,\tau_w)}{\partial \tau_w} + \frac{\partial[\omega_0(x)n_w(x,\tau_w)]}{\partial x} = 0, \tag{5.3}$$

where $n(x,\theta) = n_w(x, \mathcal{F}_w(\theta))$, and the solution of which is still given by Eq. (3.7).

In order to get the proper time parameterization, Eq. (5.2) should be inverted. Since

$$\frac{d\theta}{d\tau_w} = \frac{1}{y_A(\theta)}, \tag{5.4}$$

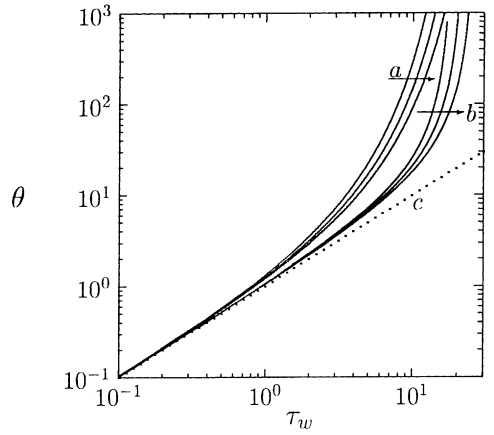

Fig. 6. Log–log plot of the physical time θ vs. the warped time τ_w for the two initial distributions I (bundle of curves a) and II (bundle of curves b) in the stoichiometric case $\gamma_A = 1$ and diffusion-controlled regime $x_D = 10^{-2}$, $x_v = 1$. The arrows indicate increasing values of the order of reaction $n = 1, 2, 3$. The dotted line (curve c) represents the linear behavior $\theta = \tau_w$.

it follows that:

$$\theta = \int_0^{\tau_w}\left\{1 - \gamma_A\left[1 - \frac{\int_0^\infty x^3 n_w(x,\tau'_w)\,dx}{\int_0^\infty x^3 n_0(x)\,dx}\right]\right\}^{-1} d\tau'_w$$
$$= \int_0^{\tau_w} \frac{d\tau'_w}{1-\gamma_A X(\tau'_w)} = \mathcal{F}_w^{-1}(\tau_w), \tag{5.5}$$

the inverse of which gives the proper relation between the warped time τ_w and the physical time θ.

The influence of the fluid reactant A depends on the parameter γ_A. While $\gamma_A = 1$ corresponds to the stoichiometric conditions of initial loading, $\gamma \to 0$ is the limit case of an overwhelming surplus of fluid reactant with respect to the solid.

Fig. 6 shows the behavior of the physical time θ vs. the warped time τ_w for the two initial distributions considered above, for different orders of reaction, and for different loading conditions (values of γ_A). The most critical case, i.e. stoichiometric loading $\gamma_A = 1$, leads to an infinite time for complete particle consumption and corresponds to the vertical asymptotes for the curves of bundles (a) and (b) in Fig. 6. Obviously, the slower the particle consumption is, the higher the value of the corresponding warped time τ_w^* at which $\theta(\tau_w)$ starts to deviate from the linear behavior $\theta = \tau_w$ (dotted curve c) corresponding to $\gamma_A = 0$. Consequently, τ_w^* increases with γ_A and is larger in the case of distribution II, characterized by an initial ensemble of large particles, and for a high value of the order of reaction n.

To conclude, there is no further peculiar complexity in approaching the case of limiting fluid reactants other than the fact that the relation between the physical time and the warped time should be enforced through Eq. (5.5).

6. Concluding remarks

This paper develops a closed-form solution of the population-balance equation expressing the dissolution of a polydisperse mixture of nonporous solid particles.

For dissolution kinetics in the presence of excess fluid reactants, the formal solution of the population balance is given by Eq. (3.7). A simple closed-form solution can be obtained in the case of a first-order kinetics for a generic initial distribution and for any values of the parameter x_D and x_v. In the more general case, e.g. for nonlinear kinetics, the expression for the auxiliary function $h(x)$ and for its inverse entering into Eq. (3.7) can be computed once and for all and the evolution of the distribution function can be obtained with arbitrary numerical accuracy by substitution into Eq. (3.7).

The influence of the physical and operating conditions is thoroughly discussed. Specifically, the mass-transfer controlled regime displays a manifold of different features that depend intrinsically on the initial particle distribution function. Essentially, mixtures of large and small particles (where "large" and "small" have a relative meaning in relation to r_{ref}), behave differently, and the dynamics of the particle mixture in the case of initially unimodular distributions can be conveniently described by means of the peak-location/conversion curve (x^* vs. X), which is also easy to obtain directly from the experimental granulometric and kinetic data.

If the bulk fluid reactant concentration does change in time, i.e. if there is not a large surplus of fluid reactant, the resulting population-balance equation becomes a nonlinear functional equation, the solution of which can still be obtained by applying Eq. (3.7) with a suitable warped-time transformation, as discussed in Section 5.

In many dissolution processes, the reaction kinetics is intertwined with particle fragmentation. The mathematical modeling of fragmentation processes leads to an integro-differential population-balance equation [21,22]:

$$\frac{\partial n(x,\theta)}{\partial \theta} + \frac{\partial[\omega(x)n(x,\theta)]}{\partial x} = -a(x)n(x,\theta) + \int_x^\infty a(y)b(x;y)n(y,\theta)\,\mathrm{d}y, \qquad (6.1)$$

where $a(x)$ is the fragmentation rate depending on the dimensionless radius x and $b(x; y)$ the number of fragments of radius x generated from a particle of radius y.

Despite the formal analogy with mechanical fragmentation, the phenomenon of particle fragmentation during chemical dissolution admits it own peculiarities, for the reason that particle break-up is essentially a consequence of the kinetics itself rather than of mechanical factors controlling grinding and milling processes. This limits the application of the existing expressions for the fragmentation functions $a(x)$ and $b(x; y)$ adopted in the description of mechanical fragmentation (abrasion, cleavage and fracture) [23,24], and of the existing closed-form solutions for Eq. (6.1), which either holds for $\omega(x) = 0$ [25,26] or applies for simplified expressions for $\omega(x)$, $a(x)$, $b(x, y)$ [21,22].

It is important to point out that a general closed-form solution for the resulting integro-differential population-balance equation occurring in dissolution fragmentation is difficult to obtain. An efficient computational way to tackle the problem is to make use of spectral (Galërkin) expansions with respect to a complete system of orthonormal basis functions [27], thus reducing the population-balance equation to a system of linear ordinary differential equations. The analysis of dissolution kinetics under fragmentation lies beyond the scope of this paper and will thus be developed elsewhere [28].

References

[1] C.Y. Wen, Noncatalytic heterogeneous solid–fluid reaction models, Ind. Eng. Chem. 60 (1969) 34.
[2] H.Y. Sohn, M.E. Wadsworth, Rate Processes of Extractive Metallurgy, Plenum Press, New York, 1979.
[3] G. Lapidus, Mathematical modelling of metal leaching in nonporous minerals, Chem. Eng. Sci. 47 (1992) 1933.
[4] Z. Ma, C. Ek, Rate processes and mathematical modelling of the acid leaching of a manganese carbonate ore, Hydrometallurgy 27 (1991) 125.
[5] M.D. Pritzker, Shrinking-core model for systems with facile heterogeneous and homogeneous reactions, Chem. Eng. Sci. 51 (1996) 3631.
[6] D.G. Dixon, The multiple convolution integral: a new method for modeling multistage continuous leaching reactors, Chem. Eng. Sci. 51 (1996) 4759.
[7] D.M. Himmelblau, K.B. Bishoff, Process Analysis and Simulation: Deterministic Systems, Wiley, New York, 1968.
[8] D. Ramkrishna, The status of population balances, Rev. Chem. Eng. 3 (1985) 59.
[9] S. Kumar, D. Ramkrishna, On the solution of population balance equations by discretization. I. A fixed pivot technique, Chem. Eng. Sci. 51 (1996) 1311.
[10] S. Kumar, D. Ramkrishna, On the solution of population balance equations by discretization. II. A moving pivot technique, Chem. Eng. Sci. 51 (1996) 1333.
[11] S. Kumar, D. Ramkrishna, On the solution of population balance equations by discretization. III. Nucleation, growth and aggregation of particles, Chem. Eng. Sci. 52 (1997) 4659.
[12] J.E. Sepulveda, J.A. Herbst, A population balance approach to the modelling of multistage continuous leaching systems, AIChE Symp. Ser. 57 (1978) 41.
[13] W.W. Stange, R.P. King, L. Woollacott, Towards more effective simulation of CIP and CIL processes. 2. A population-balance-based simulation approach, J. S. Afr. Inst. Min. Metall. 90 (1990) 307.
[14] F.K. Crundwell, A.W. Bryson, The modelling of particulate leaching reactors—the population balance approach, Hydrometallurgy 29 (1992) 275.
[15] S.E. Le Blanc, H.S. Fogler, Population balance modeling of the dissolution of polydisperse solids: rate limiting regimes, AIChE J. 33 (1987) 54.
[16] S.E. Le Blanc, H.S. Fogler, Dissolution of powdered minerals: the effect of polydispersity, AIChE J. 35 (1989) 865–868.
[17] R. Aris, Reactions in continuous mixtures, AIChE J. 35 (1989) 539.
[18] G. Astarita, Lumping nonlinear kinetics: apparent overall order of reaction, AIChE J. 35 (1989) 529.
[19] W.E. Ranz, Application of a stretch model to mixing, diffusion, and reaction in laminar and turbulent flows, AIChE J. 25 (1979) 41.

[20] R. Chella, J. Ottino, Conversion and selectivity modifications due to mixing in unpremixed reactors, Chem. Eng. Sci. 39 (1984) 551.
[21] B.F. Edwards, M. Cai, H. Han, Rate equation and scaling for fragmentation with mass loss, Phys. Rev. A 41 (1990) 5755.
[22] M. Cai, B.F. Edwards, H. Han, Exact and asymptotic scaling solutions for fragmentation with mass loss, Phys. Rev. A 43 (1991) 656.
[23] C. Varinot, S. Hiltgun, M.-N. Pons, J. Dodds, Identification of the fragmentation mechanisms in wet-phase fine grinding in a stirred bead mill, Chem. Eng. Sci. 52 (1997) 3605.
[24] P.J. Hill, K.M. Ng, Statistics of multiple particle breakage, AIChE J. 42 (1996) 1600.
[25] R.M. Ziff, E.D. McGrady, The kinetics of cluster fragmentation and depolymerisation, J. Phys. A 18 (1985) 3027.
[26] S. Hansen, J.M. Ottino, Fragmentation with abrasion and cleavage: analytical results, Powder Technol. 93 (1997) 177.
[27] R.G. Rice, D.D. Do, Applied Mathematics and Modeling for Chemical Engineers, Wiley, New York, 1995.
[28] A. Adrover, M. Giona, F. Pagnanelli, L. Toro, Modeling dissolution fragmentation in leaching processes, Unpublished.